Submitted to the 30th International Conference on High-Energy Physics ICHEP2000,
Osaka, Japan, July 2000

A Search for Squarks of R-Parity Violating SUSY at HERA

H1 Collaboration

Abstract

A search for squarks of R-parity violating supersymmetry is performed in ep collisions at HERA using H1 1994→1997 data corresponding to an integrated luminosity of 37 pb $^{-1}$. Direct single production of squarks of each generation by e^+-quark fusion via a Yukawa coupling λ' is considered and all possible R-parity violating decays and gauge decays of the squarks are taken into account. The dependence of the sensitivity to λ' on the free parameters of the Minimal Supersymmetric Standard Model (MSSM) is studied in detail. The reach in the mass-coupling plane extends to domains unexplored in other direct or indirect searches. For a Yukawa coupling of the electromagnetic strength squark masses below 258 GeV can be excluded at the 95% confidence level independently of the values of the MSSM parameters. This sensitivity still reaches 182 GeV for a 100 times smaller coupling strength. In addition, for a fixed value of the Yukawa coupling λ', HERA results are interpreted for the first time in terms of constraints on the parameters of the Minimal Supergravity model.

Abstract: 957
Parallel session: 11
Plenary talk: 7 b

1 Introduction

The ep collider HERA which provides both baryonic and leptonic quantum numbers in the initial state is ideally suited to search for new particles possessing couplings to an electron-parton pair. Such particles could be squarks, the scalar supersymmetric (SUSY) partners of the quarks, in SUSY models where R-parity is violated ($\not{R}_p$) via Yukawa couplings λ'. These squarks could thus be resonantly produced at HERA, via the fusion of the $E_e^0 = 27.5$ GeV initial state positron with a quark coming from the $E_p^0 = 820$ GeV incident proton, up to the kinematic limit of $\sqrt{s} \simeq 300$ GeV.

The interest in such new bosons coupling to an electron-parton pair has been considerably renewed recently following the observation by the H1 [1] and ZEUS [2] experiments of a possible excess of events at very high masses and squared momentum transfer Q^2, above expectations from Standard Model (SM) neutral current (NC) and charged current (CC) deep-inelastic scattering (DIS). These early results were based on data samples collected from 1994 to 1996. Of particular interest was the apparent "clustering" of outstanding NC events at masses around 200 GeV observed in H1. The mass range accessible for direct production of such "leptoquark" bosons at HERA is now severely constrained by the recent results of the TeVatron experiments [3, 4] which restrict first generation leptoquark masses at 95% confidence level to $M > 242$ GeV ($M > 205$ GeV) [5, 3] for a branching ratio β_{eq} of the new particle into $e + q$ of 1 (0.5). $\not{R}_p$SUSY provides a framework in which β_{eq} can be naturally small given the competition with gauge decay modes of the squarks, and thus leptoquark-like TeVatron constraints can be easily avoided. This strongly emphasizes the necessity [6] to perform systematic searches for squarks covering both $\not{R}_p$-decay modes and various possible gauge decay modes.

In this paper, squarks are searched through single production via a $\not{R}_p$ coupling, considering both $\not{R}_p$ decays and decays via gauge couplings involving gluinos or mixed states of gauginos and higgsinos. The analysis uses the 1994 $\rightarrow$ 1997 e^+p data corresponding to an integrated luminosity of 37 pb $^{-1}$. This represents an increase of statistics of a factor ~ 13 compared to earlier published $\not{R}_p$-violating squark searches at HERA [7, 8]. The results reported here supersede the preliminary results presented at ICHEP'98 [9] based on the same dataset.

2 Phenomenology

The most general SUSY theory which preserves gauge invariance of the Standard Model allows for Yukawa couplings between one scalar squark ($\tilde{q}$) or slepton ($\tilde{l}$) and two known SM fermions. Such couplings induce violation of the R-parity defined as $R_p = (-1)^{3B+L+2S}$, where S denotes the spin, B the baryon number and L the lepton number of the particles. $R_p = 1$ for particles and -1 for sparticles. We consider here the SUSY phenomenology at HERA in presence of $\not{R}_p$ Yukawa couplings but maintain otherwise the minimal field content of the so-called Minimal Supersymmetric Standard Model (MSSM). Of special interest for HERA are those Yukawa vertices which couple a squark to a lepton-quark pair. These are described in the superpotential by the terms $\lambda'_{ijk} L_i Q_j \bar{D}_k$, with i, j, k being generation indices [1]. The corresponding part of the Lagrangian, expanded in fields, reads as [10] :

$$\begin{aligned} \mathcal{L}_{L_i Q_j \bar{D}_k} = \lambda'_{ijk} \Big[& -\tilde{e}^i_L u^j_L \bar{d}^k_R - e^i_L \tilde{u}^j_L \bar{d}^k_R - (\bar{e}^i_L)^c u^j_L \tilde{d}^{k*}_R \\ & + \tilde{\nu}^i_L d^j_L \bar{d}^k_R + \nu_L \tilde{d}^j_L \bar{d}^k_R + (\bar{\nu}^i_L)^c d^j_L \tilde{d}^{k*}_R \Big] + \text{h.c.} \end{aligned}$$

[1] In the usual superfields notation, L_i, Q_j and $\bar{D}_k$ contain respectively the left-handed lepton doublet, quark doublet and the right handed quark singlet.

where the superscripts ^{c} denote the charge conjugate spinors and the * the complex conjugate of scalar fields. Hence, with an $e^{\pm}$ in the initial state, the couplings λ'_{1jk} allow for resonant production of squarks through $e-q$ fusion. For the nine possible λ'_{1jk} couplings, the corresponding single production processes are given in table 1. The $\tilde{u}^j_L$ ($\tilde{d}^{k*}_R$) production cross section approx-

λ'_{1jk}	production process	
111	$e^+ + \bar{u} \rightarrow \tilde{d}^*_R$	$e^+ + d \rightarrow \tilde{u}_L$
112	$e^+ + \bar{u} \rightarrow \tilde{s}^*_R$	$e^+ + s \rightarrow \tilde{u}_L$
113	$e^+ + \bar{u} \rightarrow \tilde{b}^*_R$	$e^+ + b \rightarrow \tilde{u}_L$
121	$e^+ + \bar{c} \rightarrow \tilde{d}^*_R$	$e^+ + d \rightarrow \tilde{c}_L$
122	$e^+ + \bar{c} \rightarrow \tilde{s}^*_R$	$e^+ + s \rightarrow \tilde{c}_L$
123	$e^+ + \bar{c} \rightarrow \tilde{b}^*_R$	$e^+ + b \rightarrow \tilde{c}_L$
131	$e^+ + \bar{t} \rightarrow \tilde{d}^*_R$	$e^+ + d \rightarrow \tilde{t}_L$
132	$e^+ + \bar{t} \rightarrow \tilde{s}^*_R$	$e^+ + s \rightarrow \tilde{t}_L$
133	$e^+ + \bar{t} \rightarrow \tilde{b}^*_R$	$e^+ + b \rightarrow \tilde{t}_L$

Table 1: Squark production processes at HERA (e^+ beam) via a R-parity violating λ'_{1jk} coupling.

imately scales as $\lambda'^2_{1jk} \times d^k(x)$ ($\bar{u}^j(x)$) where $d^k(x)$ ($\bar{u}^j(x)$) are the probabilities to find a quark d^k ($\bar{u}^j$) in the proton with a momentum fraction $x = M^2_{\tilde{q}}/s$; $M_{\tilde{q}}$ denotes the squark mass and $\sqrt{s}$ is the available energy in the ep centre of mass frame. With an e^+ incident beam, HERA is best sensitive to couplings λ'_{1j1}, where mainly $\tilde{u}^j_L$ squarks could be produced via processes involving a valence d quark. On the contrary, HERA e^-p data taken in 1998-1999 will allow to better probe couplings λ'_{11k} and $\tilde{d}^k_R$ squarks.

In this paper, squarks are searched under the simplifying assumptions that one of the λ'_{1jk} dominates[2]. The squarks decay either via their Yukawa coupling into SM fermions, or via their gauge couplings into a quark and a neutralino χ^0_i ($i = 1, 4$), a chargino χ^+_j ($j = 1, 2$), or a gluino $\tilde{g}$. The mass eigenstates χ^0_i and χ^+_j are mixed states of gauginos and higgsinos and, as the $\tilde{g}$, are in general unstable. This latter point holds in $\not{R}_p$ SUSY also for the Lightest Supersymmetric Particle (LSP) which decays via λ'_{1jk} into a quark, an antiquark and a lepton [10]. This is in contrast to R_p conserving SUSY models and has important phenomenological and possibly cosmological consequences.

In cases where both production and decay occur through a λ'_{1jk} coupling (e.g. Fig. 1a and c for $\lambda'_{1j1} \neq 0$), the squarks behave as scalar leptoquarks [12]. The $\tilde{d}^{k*}_R$ can decay either into $e^+ + \bar{u}^j$ or $\nu_e + \bar{d}^j$ while the $\tilde{u}^j_L$ only decays into $e^+ + d^k$ by gauge invariance. Hence, the final state signatures consist of a lepton and a jet and are, event-by-event, indistinguishable from the SM neutral and charged current DIS.

In cases where the $\tilde{u}^j_L$ (resp. $\tilde{d}^{k*}_R$) undergoes a gauge decay into a χ^0_α, a χ^+_β or a $\tilde{g}$ (resp. a χ^0_α or a $\tilde{g}$) (e.g. Fig. 1b and d) the final state will depend on the subsequent decay of the SUSY fermion. Neutralinos can undergo the $\not{R}_p$ decays $\chi^0_\alpha \rightarrow e^{\pm}q\bar{q}'$ or $\chi^0_\alpha \rightarrow \nu q\bar{q}$, the former (latter) being dominant if χ^0_α is dominated by its photino (zino) component. Gluinos can undergo the same $\not{R}_p$decays, both modes being equally probable if the squarks of j^{th} and k^{th} generation are degenerate. When a χ^0_α or a $\tilde{g}$ decays via $\not{R}_p$ into a charged lepton, both the "right" and

[2]The case where products of couplings $\lambda'_{1jk} \times \lambda'_{3jl}$ or $\lambda'_{1jk} \times \lambda'_{2jl}$ are non vanishing has been addressed in [11] where a search for Lepton Flavor Violation is presented.

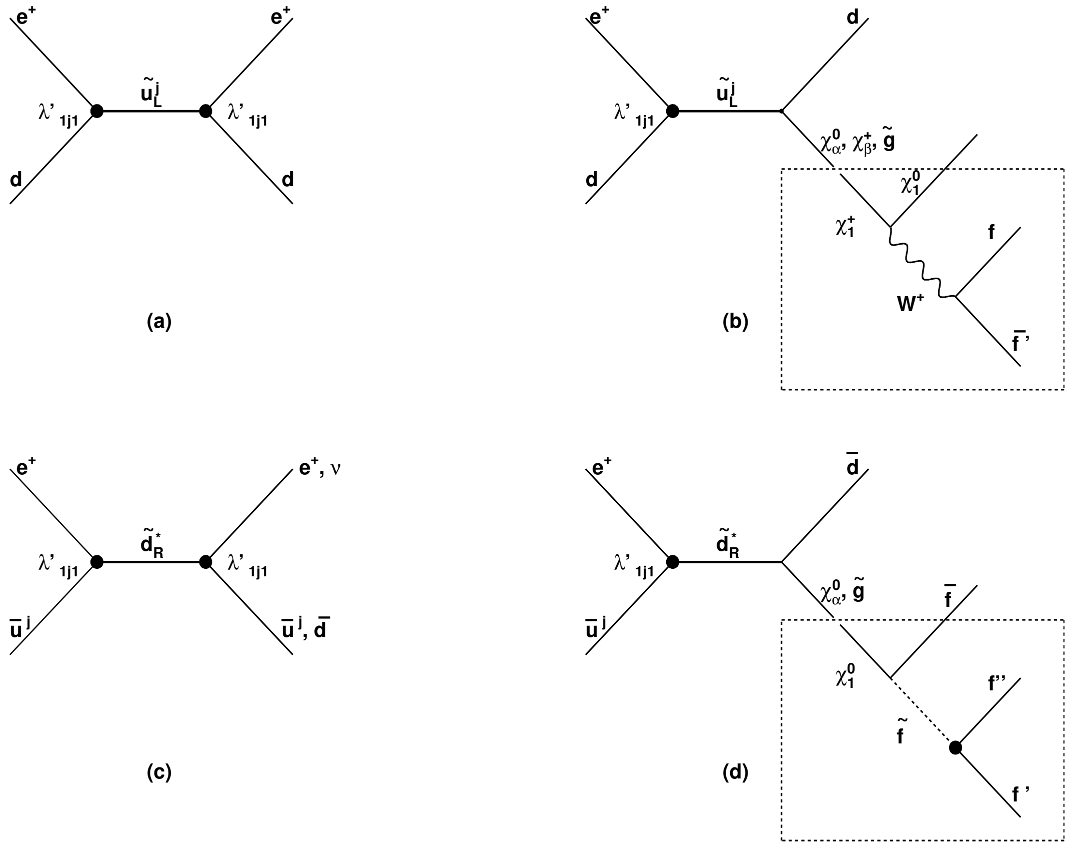

Figure 1: Lowest order s-channel diagrams for $R\!\!\!/_p$squark production at HERA followed by (a),(c) $R\!\!\!/_p$ decays and (b),(d) gauge decays of the squark. In (b) and (d), the emerging neutralino, chargino or gluino might subsequently undergo a R_p violating or R_p conserving decay of which examples are shown in the dashed boxes for (b) the χ_1^+ and (d) the χ_1^0.

the "wrong" sign lepton (compared to incident beam) are equally probable leading to largely background free striking signatures for lepton number violation. On the contrary, the only $R\!\!\!/_p$ decays for charginos are $\chi_\alpha^+ \rightarrow \nu u^j \bar{d}^k$ and $\chi_\alpha^+ \rightarrow e^+ d^k \bar{d}^j$. Neutralinos χ_α^0 with $\alpha > 1$ as well as charginos (resp. gluinos) can also undergo gauge decays into a lighter χ and two SM fermions (resp. two quarks), through a real or virtual gauge boson or sfermion (resp. squark). Radiative decays of a heavy χ into a photon or a Higgs boson and a lighter χ can also occur in particular cases.

The possible decay chains of the $\tilde{u}_L^j$ and $\tilde{d}_R^{k*}$ analysed in this paper are classified into eight distinguishable event topologies described in table 2, and are labeled S1 to S8 following the notation introduced in [8]. This classification relies on the number of charged leptons and/or jets in the final state, and on the presence of missing energy. Channels S1 and S2 are the "leptoquark-like" decay modes of the squark, proceeding directly via $R\!\!\!/_p$. Channels S3 to S5 involve one or two SUSY fermion(s) denoted by X and Y in table 2. As mentioned already only a neutral SUSY fermion (a χ_α^0 or a $\tilde{g}$) can be involved in the last step of a S4 decay. Channels S7 and S8 necessarily involve two SUSY fermions. In the case where the χ_1^0 has a very small decay width, such that it would decay outside the detector (i.e. when it is nearly a pure mixture of Higgsinos) the cascade decay of a squark into a chargino, followed by $\chi^+ \rightarrow l^+ \nu_l \chi_1^0$, would lead to an event topology which has been analysed previously in [8] and labeled S6. Since the region of the MSSM parameter space which would allow a χ^0 to escape detection has now been ruled out by recent results from LEP2 [13], this channel has not been considered here. Decay patterns involving more than two χ or $\tilde{g}$ are in general kinematically suppressed and are not considered in the analysis. The relative contributions of the channels S1 to S8 depend in particular on the value of the Yukawa coupling λ' and on the gaugino-higgsino mixture of neutralinos and charginos. They will be shown as a function of the squark mass in section 6.2 for some example cases.

Channel	Decay processes	Signature
S1	$\tilde{q} \xrightarrow{\lambda'} e^+ \quad q$	High P_T e^+ + 1 jet
S2	$\tilde{d}^*_R \xrightarrow{\lambda'} \nu_e \quad \bar{d}$	Missing P_T + 1 jet
S3	$\tilde{q} \longrightarrow q \quad X$ $\overset{\lambda'}{\hookrightarrow} \quad e^+\bar{q}q$ $\tilde{q} \longrightarrow q \quad X$ $\hookrightarrow \quad q\bar{q} \quad Y$ $\overset{\lambda'}{\hookrightarrow} e^+\bar{q}q$	e^+ + multiple jets
S4	$\tilde{q} \longrightarrow q \quad \chi^0_\alpha, \tilde{g}$ $\overset{\lambda'}{\hookrightarrow} \quad e^-\bar{q}q$ $\tilde{q} \longrightarrow q \quad X$ $\hookrightarrow \quad q\bar{q} \quad Y$ $\overset{\lambda'}{\hookrightarrow} e^-\bar{q}q$	e^- (i.e. wrong sign lepton) + multiple jets
S5	$\tilde{q} \longrightarrow q \quad X$ $\overset{\lambda'}{\hookrightarrow} \quad \nu(\bar{\nu})\bar{q}q$ $\tilde{q} \longrightarrow q \quad X$ $\hookrightarrow \quad q\bar{q} \quad Y$ $\overset{\lambda'}{\hookrightarrow} \nu(\bar{\nu})\bar{q}q'$	Missing P_T + multiple jets
S7	$\tilde{q} \longrightarrow q \quad X$ $\hookrightarrow \quad l\nu_l \quad Y$ $\overset{\lambda'}{\hookrightarrow} e^\pm\bar{q}q$	e + e or μ + Missing P_T + multiple jets
S8	$\tilde{q} \longrightarrow q \quad X$ $\hookrightarrow \quad l\nu_l \quad Y$ $\overset{\lambda'}{\hookrightarrow} \nu\bar{q}q$	e or μ + Missing P_T + multiple jets

Table 2: Squark decay channels in $\not{R}_p$ SUSY classified per distinguishable event topologies. Only the final states which are analysed here are listed in the table. X and Y denote a gluino, a neutralino or a chargino, and quarks are generically denoted by q.

3 The H1 detector

A detailed description of the H1 detector can be found in [14]. Here we describe only the components relevant for the present analysis in which the final state of the events involves either a positron[3] with high transverse energy or a large amount of hadronic transverse energy flow.

The positron energy and angle are measured in a liquid argon (LAr) sampling calorimeter [15] covering the polar angular[4] range $4^\circ \leq \theta \leq 154^\circ$ and all azimuthal angles. The granularity is optimized to provide fine and approximately uniform segmentation in laboratory pseudorapidity and azimuthal angle ϕ. It consists of a lead/argon electromagnetic section followed by a stainless steel/argon hadronic section. Electromagnetic shower energies are measured with a resolution of $\sigma(E)/E \simeq 12\%/\sqrt{E/\text{ GeV}} \oplus 1\%$ and pion induced hadronic energies with $\sigma(E)/E \simeq 50\%/\sqrt{E/\text{ GeV}} \oplus 2\%$ after software energy weighting. These resolutions were measured in test beams with electron energies up to 166 GeV [16, 17] and pion energies up to 205 GeV [17]. The energy calibration was determined initially from test beam data with an uncertainty of 3% and 4% for electromagnetic and hadronic energies respectively. A new absolute energy scale calibration for positrons detected in the actual H1 experiment has been recently established [18] *in situ* by using the over-constrained kinematics of NC DIS, QED Compton and e^+e^- pair production from two-photons processes. A precision of 0.7% is reached in the LAr central barrel region $80^\circ \lesssim \theta_e \lesssim 145^\circ$, 1.5% in $40^\circ \lesssim \theta_e \lesssim 80^\circ$ and 3.0% in the forward region $5^\circ \lesssim \theta_e \lesssim 40^\circ$. This represents an improved understanding of the electromagnetic energy scale compared to [1], made possible by the increase of statistics accumulated in 1997. All analyses described in the following rely on this updated calibration. The angular resolution on the positron measured from the electromagnetic shower in the calorimeter varies from ~ 2 mrad below 30° to $\lesssim 5$ mrad at larger angles. A lead/scintillating-fibre backward calorimeter [19] extends the coverage[5] at larger angles ($153^\circ \leq \theta \lesssim 178^\circ$).

Surrounded by the calorimeters is the tracking system which is used here to determine the position of the interaction vertex. The main components of this system are central drift and proportional chambers ($25^\circ \leq \theta \leq 155^\circ$), a forward track detector ($7^\circ \leq \theta \leq 25^\circ$) and a backward drift chamber[5]. The tracking chambers and calorimeters are surrounded by a superconducting solenoid providing a uniform field of 1.15 T parallel to the z axis within the detector volume. The instrumented iron return yoke surrounding this solenoid is used to measure leakage of hadronic showers and to recognize muons. In the very forward region ($\theta \leq 15^\circ$) muons can also be detected in three double layers of drift chambers, forming the Forward Muon Detector (FMD). The luminosity is determined from the rate of Bethe-Heitler $ep \to ep\gamma$ bremsstrahlung events measured in a luminosity monitor. This consists of a positron tagger (e-tagger) and a photon tagger (γ-tagger), located -33 m and -103 m respectively from the interaction point, respectively.

For the acquisition of events we rely on the timing information from a time-of-flight system and on the LAr trigger system which provides a measurement of the energy flow using coarse trigger towers [15].

4 Monte Carlo Event Generators

A complete Monte Carlo simulation of the H1 detector response is performed for each possible background source.

[3]Unless otherwise stated, the analysis does not distinguish explicitly between e^+ and e^-.

[4]The z axis is taken to be in the direction of the incident proton, and the origin of coordinates is the nominal ep interaction point.

[5]The detectors in the backward region were upgraded in 1995 by the replacement of the lead/scintillator tile calorimeter [20] and a proportional chamber.

For the NC or CC DIS background estimates we use the DJANGO [21] event generator, which includes first order QED radiative corrections. Simulation of real bremsstrahlung photons, based on HERACLES [22], is also included. QCD radiation at all orders is treated following the approach of the Color Dipole Model [23] and is implemented using ARIADNE [24]. The hadronic final state is generated using the string fragmentation model [25]. The parton densities in the proton used to estimate DIS expectations are taken from the MRST [26] parametrization.

For direct and resolved photoproduction of light and heavy flavours, we use the PYTHIA MC event generator [27] which relies on first order QCD matrix element and uses leading-log parton showers and string fragmentation [25]. The GRV LO (GRV-G LO) parton densities [28] in the proton (photon) are used at low Q^2.

The simulation of the leptoquark-like signatures ($\mathrm{S1}$ and $\mathrm{S2}$ topologies) relies on the event generator LEGO [29] which is described in more detail in [30]. For squarks undergoing gauge decays, we use the SUSYGEN [31] event generator, recently extended [32, 33] to allow to generate SUSY events in ep and hadronic collisions. Any gauge decay for the resonant squark can be generated, and the cascade decay of the subsequent χ's or $\tilde{g}$ are performed according to the corresponding matrix elements.

In both LEGO and SUSYGEN initial and final state parton showers are simulated following the DGLAP [34] evolution, and string fragmentation [27, 25] is used for the non-perturbative part of the hadronization. In addition initial state bremsstrahlung in the collinear approximation is simulated in the LEGO generator. The parton densities used [26] are evaluated at the scale of the squark mass. This scale is also chosen for the maximum virtuality of parton showers initiated by a quark coming from the squark decay. Moreover in the SUSYGEN generator the parton showers modeling QCD radiation off quarks emerging from a χ or $\tilde{g}$ decay are started at a scale given by the mass of this SUSY fermion.

Many samples of events corresponding to final states $\mathrm{S1}$ to $\mathrm{S8}$ have been generated and were passed through a complete simulation of the H1 detector. The squark mass for these simulations has been varied from 75 GeV to 275 GeV in steps of $\simeq 25$ GeV. Gauge decays of squarks involving one or two SUSY fermion have been simulated separately. For gauge decays of squarks into a χ^0 or χ^+ which directly decays via $\not{R}_p$(i.e. processes corresponding to the first line of the $\mathrm{S3}$, $\mathrm{S4}$ and $\mathrm{S5}$ slots in table 2) the process $\tilde{q} \rightarrow q\chi_1^0$ has been simulated, for χ_1^0 masses ranging between ~ 40 GeV and ~ 160 GeV. In order to study gauge decays involving two SUSY fermions (this is in particular the case for squarks decays into gluinos), the process $\tilde{q} \rightarrow q\chi_1^+ \rightarrow q\chi_1^0 f\bar{f}'$ has been simulated for χ_1^+ masses ranging between ~ 90 GeV and $\sim M_{\tilde{q}} - 20$ GeV, and for χ_1^0 masses between $\sim$ half of the χ_1^+ mass and $\sim M(\chi_1^+) - 20$ GeV. Masses of the χ's were varied by steps of ~ 20 GeV. These simulations allowed to determine signal selection efficiencies as a function of the masses of the squark and of the involved SUSY fermion(s) for essentially all allowed scenarios. The relatively fine grid of simulated scenarios permits to interpolate linearly between them, and extrapolate for points in the parameter space slightly outside the simulated region.

5 Analysis

The data reduction starts by the rejection of non-colliding background. It is common to all channels presented below and requires that the event survives a set of halo and cosmic muon filters, and that it is properly in time relative to interacting bunch crossings. Moreover, a primary interaction vertex must be reconstructed in the range $\mid z - \bar{z} \mid < 40$ cm where the mean position $\bar{z}$ of the nominal interaction point varies between ± 5 cm around $z = 0$ depending on the HERA beam settings. Moreover the events must have been accepted by a LAr trigger asking either for an electromagnetic cluster, for a large transverse energy in the central part of the calorimeter, or for a large imbalance in the transverse energy flow.

In what follows, unless explicitly stated otherwise, the energy flow summations run over all energy deposits i in the calorimeters (apart from the electron and photon taggers). Thus, the missing transverse momentum $P_{T,miss}$ is obtained as $P_{T,miss} \equiv \sqrt{\left(\sum E_{x,i}\right)^2 + \left(\sum E_{y,i}\right)^2}$ with $E_{x,i} = E_i \sin\theta_i \cos\phi_i$ and $E_{y,i} = E_i \sin\theta_i \sin\phi_i$. The momentum balance with respect to the incident positron is obtained as $\sum(E - P_z) \equiv \sum(E_i - E_{z,i})$ with $E_{z,i} = E_i \cos\theta_i$. $\sum(E - P_z)$ should peak at $2E_e^0$ for events where only particles escaping in the proton direction remain undetected.

5.1 Event Selection for topology S1

Squarks decaying via S1 behave as scalar leptoquarks and are characterized by NC DIS-like signatures. The scattered positron is expected to have a high transverse energy $E_{T,e}$ due to the Jacobian peak at $M_{\tilde{q}}/2$ of the $E_{T,e}$ distribution. The squark mass is related to the usual Bjorken x via $M = \sqrt{xs}$. Squarks being scalar particles, they decay isotropically in their centre of mass (CM) frame. Hence, the usual DIS Bjorken scattering variable y, which is related to the positron polar angle θ_e^* in the $e - q$ CM frame via $y = (1 + \cos\theta_e^*)/2$, is uniformly distributed for such events. This contrasts with the steeply falling $1/y^2$ dependence expected for NC DIS at fixed mass (i.e. fixed x). Hence the strategy is to look for resonances in NC DIS-like events at high M and high y, i.e. at high Q^2. The selection criteria are those described in [11] where a search for leptoquarks based on the data used here is presented in detail. The main selection criteria are the following :

1. an isolated positron with $E_{T,e} > 15$ GeV found in the LAr calorimeter; the positron energy cluster should contain more than 98% of the LAr energy found within a pseudorapidity-azimuthal cone of opening $\sqrt{(\Delta\eta_e)^2 + (\Delta\phi_e)^2} = 0.25$ where $\eta_e = -\ln\tan\frac{\theta_e}{2}$; at least one charged track is required within the positron isolation cone;
2. a total transverse momentum balance $P_{T,miss}/\sqrt{E_{T,e}} \leq 4\sqrt{\text{GeV}}$;
3. a limited reconstructed momentum loss in the direction of the incident positron such that $40 \leq \sum(E - P_z) \leq 70$ GeV.

The cut (2) maintains a high selection efficiency for NC DIS-like events up to the highest $E_{T,e}$, by taking into account the natural scale of the hadronic energy resolution for e + jet events. Cut (3) provides a powerful rejection of photoproduction contamination and also suppresses NC DIS-like events with a very hard γ emitted from the initial state positron. Moreover the analysis is restricted to the kinematic domain $Q^2 > 2500$ GeV^2 and $0.1 < y < 0.9$. We use here the measurement of the scattered positron energy and angle to reconstruct the variables M, y and Q^2, henceforth labeled M_e, y_e and Q_e^2. Kinematic formulae can be found in [11].

The signal significance is then optimized by applying in addition a M_e dependent y_e cut [11]. This y_e cut varies from $y_e \gtrsim 0.6$ at 60 GeV to $y_e \gtrsim 0.4$ at 200 GeV and down to $y_e \gtrsim 0.2$ around 260 GeV. We observe 310 events satisfying all the above requirements in the mass range $M_e >$

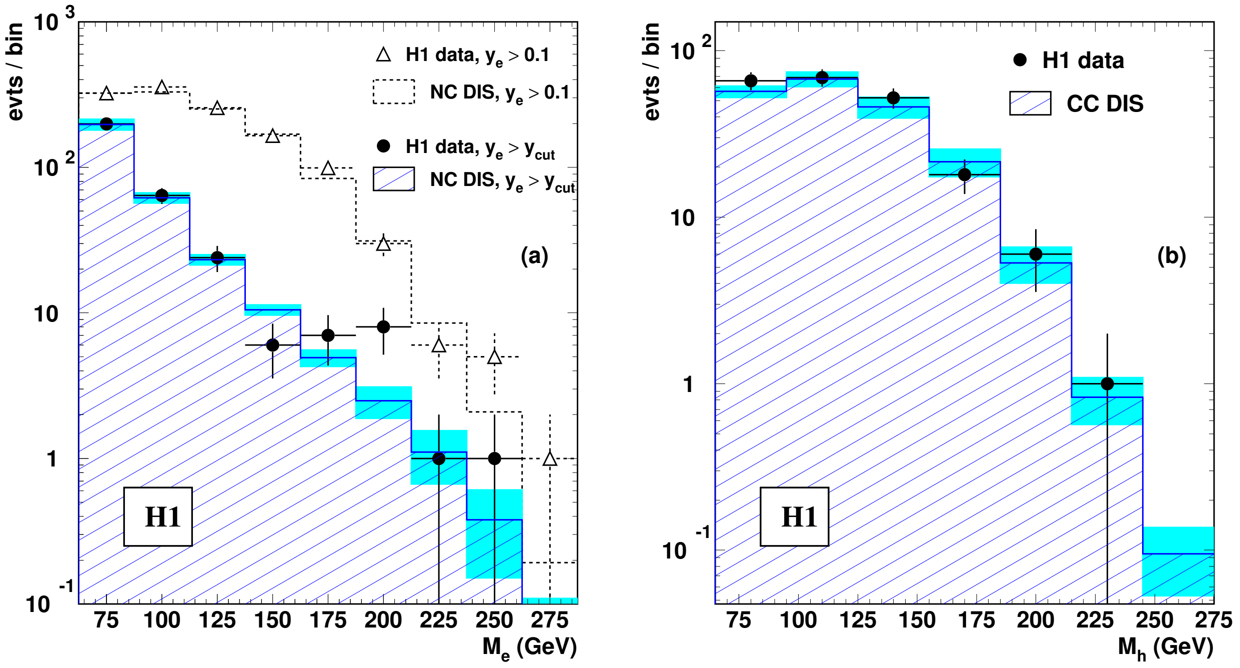

Figure 2: Mass spectra for (a) NC DIS-like and (b) CC DIS-like final states for data (symbols) and DIS expectation (histograms). In (a), the NC DIS-like comparison is shown before (open triangles, white histogram) and after (closed dots, hatched histogram) a y cut designed to maximize the significance of an eventual scalar LQ signal. The gray boxes indicate the $\pm1\sigma$ band combining the statistical and systematic errors of the NC and CC DIS expectations.

62.5 GeV, which is in good agreement with the SM expectation of 301.2 ± 22.7 (the sources of systematic errors will be described in section 5.5). The measured mass spectrum of these candidates is compared to the NC DIS expectation in Fig. 2a. The observed mass spectrum is seen to be well described by the SM expectation, with nevertheless a slight excess in the mass range 200 GeV $\pm\, \Delta M/2$ with $\Delta M = 25$ GeV, where 8 events are observed while 2.87 ± 0.48 are expected. This "clustering" is however less significant than that observed with $94 \rightarrow 96$ data alone [1]. This figure also shows the important background reduction achieved when applying the optimized y_{cut} instead of the fixed cut $y_e > 0.1$.

For this channel, the $R\!\!\!/_p$ SUSY signal detection efficiency is found to vary between $\simeq 40\%$ and $\simeq 75\%$ for squark masses ranging from 75 to 275 GeV.

5.2 Event Selection for topology S2

Squarks undergoing $\mathrm{S2}$ decays lead to CC DIS-like signatures with high missing transverse momentum due to the high E_T escaping neutrino. In contrast to the $\mathrm{S1}$ channel only $\tilde{d}_R^{k*}$ squarks, produced via a fusion between the incident e^+ and a $\bar{u}^j$ quark from the proton, can undergo such a decay. HERA sensitivity with an e^+ incident beam is thus lowered in this channel since a high x sea quark must participate in the fusion. The analysis performed to search for such leptoquarks and described in [11] is also relevant to seek squarks decaying via $\mathrm{S2}$. Hence only the main cuts and results are presented here. The $\mathrm{S2}$ selection mainly requires :

1. no $e^{\pm}$ candidate with $E_T > 5$ GeV found in the LAr calorimeter, using the same electron identification algorithm as used for S1;

2. a missing transverse momentum $P_{T,miss} > 30$ GeV.

These cuts eliminate NC DIS and photoproduction backgrounds. As for the S1 channel, we concentrate on the high Q^2 domain by requiring $Q_h^2 > 2500$ GeV^2. The kinematic variables are here reconstructed using the Jacquet-Blondel ansatz [35] by summing over all measured final state hadronic energy deposits, and in that case are labeled M_h, y_h and Q_h^2. Kinematic formulae can be found in [11]. We also require $y_h < 0.9$ to avoid the high y_h domain where the resolution on the mass $M_h = \sqrt{x_h s}$ reconstructed from the hadronic energy flow becomes poor [1].

We observe 213 events satisfying these requirements in the mass range $M_h > 50$ GeV, which agrees well with the CC DIS expectation of 199.1 ± 11.5. The observed and expected mass spectra are shown to be in good agreement in Fig. 2b.

The $\not{R}_p$ SUSY signal detection efficiency in this channel, determined from Monte-Carlo, varies between $\simeq 32\%$ for a 75 GeV squark mass to $\simeq 79\%$ at 275 GeV. In the lowest mass range the efficiency is limited due to the high $P_{T,miss}$ requirement.

5.3 Selection for e + jets + X topologies

When the squark undergoes a gauge decay leading to a positron, the final states can be classified into several topologies, namely S3, S4, S7e, S7μ and S8e. The selection requirements which are common to all these e + multijets channels are the following :

1. one positron candidate in the angular range $5° < \theta_e < 110°$ with $E_{T,e} > 5$ GeV, using the same positron identification criteria as used for S1;

2. at least two jets in the angular range $7° < \theta < 145°$ and with $E_T > 10$ GeV; these are found using a cone algorithm in the laboratory frame with a radius $\sqrt{\Delta\eta^2 + \Delta\phi^2} = 1$; moreover, the highest P_T jet is required to satisfy $\theta > 10°$ and $E_T > 15$ GeV;

3. the y variable reconstructed using the energy and polar angle of the highest E_T e should satisfy $y_e > 0.4$;

4. the jet among the two highest P_T jets selected as explained above, for which the polar angle $\theta_{backward}$ is maximal should verify :

$$y_e - 0.4 > (\theta_{backward} - 25°) \times (0.9 - 0.4)/(145 - 25).$$

5. the minimum of the polar angles of the highest E_T positron and of the two highest E_T jets should verify

$$\theta_{min} = Min(\theta_e, \theta_{j,1}, \theta_{j,2}) < 45°$$

For events where a positron comes from the gauge decay of a squark, the scattered e arises from the decay of the last χ or $\tilde{g}$ appearing in the decay chain and it only takes away a fraction of the momentum of this fermion. Hence its energy can be quite small and the cut applied on $E_{T,e}$ is lower than that used in the S1 analysis, in order to maintain a high enough efficiency for the searched signal. Moreover, final state e's coming from a squark cascade decay are strongly boosted in the direction of the incident proton, such that the $\theta_e < 110^\circ$ requirement discriminates powerfully the signal from NC DIS background. Cut (3), by selecting high y_e events, strongly suppresses NC DIS background while retaining high efficiency for the signal. Indeed, the $y_e = 1 - E_e/E_e^0 \sin^2(\theta_e/2)$ distribution reconstructed from the measurement of the scattered e appears strongly shifted towards large y_e in SUSY events for the reasons given above. Cut (4) exploits the fact that, for high y_e NC DIS events satisfying the above set of cuts, one hard jet is usually scattered in the backward region of the calorimeter. On the contrary, jets coming from a squark gauge decay will be boosted in the forward direction, independently of y_e. The effect of this cut and how it separates the signal from the remaining NC DIS background is illustrated in Fig. 3. In Fig. 3a, several sets of $(M_{\tilde{q}}, M_\chi)$ are combined. The effect of cut (4) on signal events depends on the masses of the involved sparticles but retains a high efficiency over the whole range considered here. Cut (5) requires that one of the squark decay products

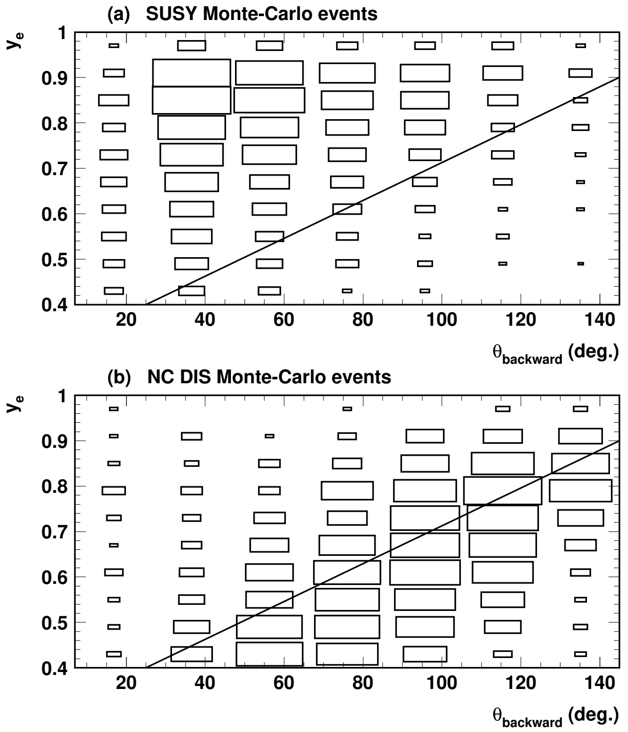

Figure 3: *Correlation between the y_e variable reconstructed from the e measurement and the angle $\theta_{backward}$ of the most backward jet for (a) SUSY Monte-Carlo events in which the squark undergoes a gauge decay leading to e + multijets $+X$ final states and (b) NC DIS Monte-Carlo events, when preselection cuts (1) to (3) are applied. Cut (4) only retains events above the diagonal line.*

should be emitted in the forward direction and allows an additional reduction of $\sim 40\%$ of the SM background, with a negligible efficiency loss on the signal.

Applying all the above selection criteria, 214 events are accepted, which is in good agreement with the SM prediction of 209.9 ± 33.7, including 47.3 expected events from photoproduction where e.g. a jet has been misidentified as an electron. Fig. 4 shows for these candidates the distributions of the transverse energy of the highest E_T positron, y_e, the transverse momentum of the most forward and most backward jet, the polar angle of the most backward jet, and the missing transverse momentum. All distributions are seen to be well described by the SM expectation. In particular, the high y_e domain dominated by misidentified photoproduction events is well under control.

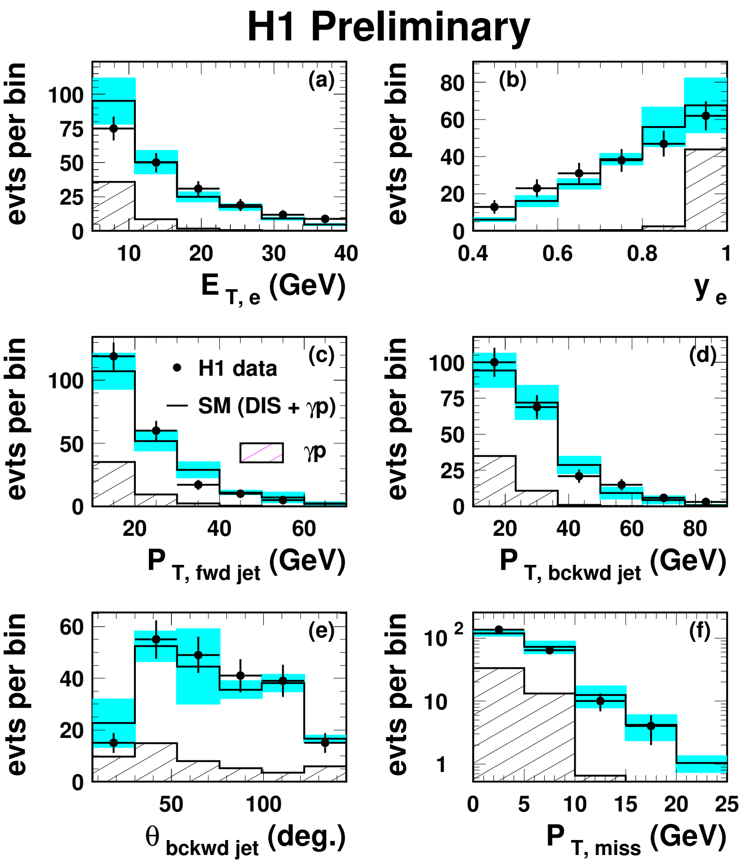

Figure 4: *For the* e + *multijets* $+X$ *preselected events, distributions of (a) the transverse energy* $E_{T,e}$ *of the highest* E_T *positron; (b)* y_e*; (c) the transverse momentum of the most forward jet; (d) the transverse momentum of the most backward jet; (e) the polar angle* $\theta_{backward}$ *of the most backward jet; (f) the missing transverse momentum. Superimposed on the data points (symbols) are histograms of the SM expectation (DIS and* γp*). The gray band indicates the uncertainty on the SM prediction. The contribution from* γp *processes alone is shown as the hatched histogram.*

5.3.1 Event Selection for topology S3

For gauge decays of squarks leading to a "right" sign final state lepton (e.g. $e^+q' \to \tilde{q} \to \chi_1^0 + q \to e^+q''\bar{q}''q'$) we require, in addition to the preselection requirements listed previously :

1. a total transverse momentum balance $P_{T,miss} < 20$ GeV;
2. $40 \leq \sum(E - P_z) \leq 70$ GeV.

We find 160 candidates satisfying the above set of cuts, which is in good agreement with the mean SM background of 152.6 ± 13.4 expected from NC DIS and photoproduction.

An invariant mass M_{inv} is then calculated using the energy $E_{wrm} = \sum_i E_i$ where the sum runs over all energy deposits in the calorimeters at $\theta > 10°$ in order to exclude the proton remnant. Ideally the squark mass should be equal to $\sqrt{4xE_e^0E_{wrm}}$. Bad measurements of

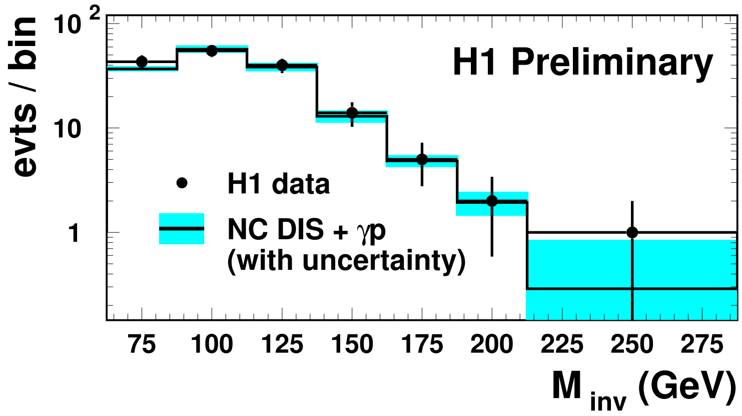

Figure 5: *Mass spectrum for e + multijets final states (event topology S3) for data (symbols) and NC DIS expectation (histogram). The gray band indicates the uncertainty of the SM prediction.*

the hadronic flow can alter this relation, and the variable $\sum(E - P_z)$ is used to estimate the induced under- or over-estimation of the squark mass, which is thus reconstructed as :

$$M_{inv} = \sqrt{4xE_e^0 E_{wrm}} - \frac{\sum(E - P_z) - 2E_e^0}{2}$$

This reconstruction method improves the peak mass resolution for squarks decaying via S3 by a factor $\simeq 2$ compared to H1 previous published analysis [8], this resolution being typically 7 GeV for a 200 GeV squark mass.

The measured mass spectrum of the S3 selected events is shown in Fig. 5 to be well described by the SM prediction. The previous analysis [8] using only 1994 e^+p data showed a slight excess (2.9σ) in the invariant mass spectrum for masses around 80 GeV. This is clearly not confirmed with the additional statistics analysed here.

In this channel, the $\not{R}_p$ SUSY signal detection efficiency depends mainly on the mass of the SUSY fermion(s) entering the decay chain. Note that experimentally the efficiencies for $right\,sign$ and for $unsigned$ events are summed. Typical values are $\simeq 50\%$ for a 200 GeV squark decaying into a 80 GeV χ_1^0, and $\simeq 35\%$ when these masses are set respectively to 100 GeV and 40 GeV.

5.3.2 Event Selection for topology S4

For a gauge decay of the squarks leading to a "wrong" sign final state lepton (i.e. $e^+q' \rightarrow \tilde{q} \rightarrow e^-q''\bar{q}''q'$) we apply the same requirements as for channel S3 and perform a determination of the lepton charge using the tracking chamber information.

We consider the track which, among the vertex fitted tracks found in the electron isolation cone, has the highest momentum projected on the axis defined by the event vertex and the centre of gravity of the calorimetric energy deposits associated to the electron. This track is required to correspond to a negatively charged particle and must moreover satisfy the following criteria :

1. the track momentum P must match the calorimetric energy E_e of the e candidate within : $P/E_e > 0.5$;
2. the error on the track curvature κ must verify $\mid \kappa/\delta\kappa \mid > 2$.

These cuts ensure a good quality of the track reconstruction at the expense of a reduced efficiency. We found that the fraction of S3 selected candidates which fulfill these additional requirements is $\simeq 80\%$, which is well reproduced by the NC DIS simulation. We thus rely on the SUSY Monte-Carlo to estimate the efficiency loss of the above cuts (1) and (2) on the signal.

No wrong sign candidate is observed in the data, while the SM prediction as estimated from Monte-Carlo is 1.3 ± 0.3 (coming from NC DIS).

5.3.3 Event Selection for topology S7, e channel (S7e)

For gauge decays of squarks leading to several jets and two e's in the final state, we require, in addition of the common preselection cuts listed previously :

1. a second e candidate, again in the angular range $5° < \theta_e < 110°$ and with $E_{T,e} > 5$ GeV, using the same positron identification criteria as used for S1.

We observe no candidate satisfying this additional cut for an expectation of 0.7 ± 0.1 event from NC DIS processes.

These criteria ensure a typical selection efficiency of $\sim 30\%$ on the searched signal.

5.3.4 Event Selection for topology S7, μ channel (S7μ)

The second possibility for a S7 topology is that the second lepton in the final state is a muon. We search for this signature by applying exactly the same cuts as for S7e, but instead of a second electron we require a muon candidate in the polar angular range of $10° < \theta < 110°$ with a transverse momentum $p_T^\mu > 5$ GeV.

A muon candidate is identified by a track, well measured in the central or forward tracking system. In the overlap region information from both tracking systems is combined. The track has to match geometrically an energy deposition in the LAr calorimeter, compatible with that expected from a minimum ionizing particle, and/or a track in the instrumented iron and/or a track in the forward muon detector. The muon properties were found to be well described by the simulation, as shown in Fig. 6 for the example of the p_T^μ distribution.

Depending on the masses of the supersymmetric particles the muon is not necessarily of very high p_T. Furthermore the muons are not necessarily expected to be well isolated. Hence we are not requiring any isolation criterion and the cut on $p_T^\mu > 5$ GeV was chosen analogous to the S7e selection but was independently found to be optimal concerning the signal to background ratio.

The final selection efficiency for the S7μ signal is between 35 and 50% for most of the SUSY parameter space.

After this selection we observe 2 candidates where 4.2 ± 1.2 are expected for SM processes (3.0 from NC DIS and 1.2 from photoproduction).

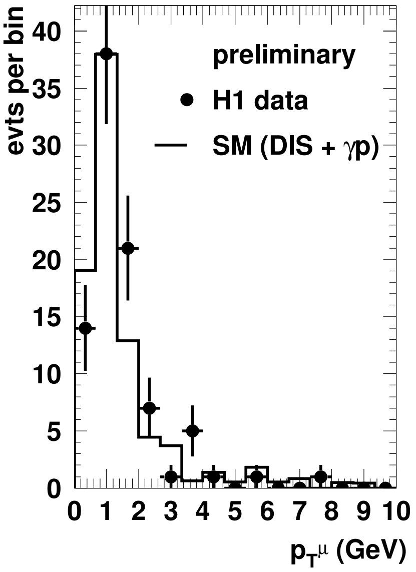

Figure 6: *Distribution of the transverse momentum p_T^μ of the muon for events satisfying the common preselection criteria and where a muon has been identified in addition, for data (points) and SM MC (histogram). The muon is required to be in the polar angular range of* $10° < \theta < 110°$.

5.3.5 Event Selection for topology S8, e channel (S8e)

For gauge decays of squarks leading to e + multijets + $P_{T,miss}$ final states, we require in addition to the common preselection criteria :

1. a missing transverse momentum $P_{T,miss} > 15$ GeV ;
2. that the variables y_e (see section 5.1) and y_h (see section 5.2) verify : $y_e \times (y_e - y_h) > 5\%$.

Cut (2) exploits the fact that, for events coming from a squark decaying via S8e, the escaping neutrino carries away a non-negligible part of $E - p_z$ leading the variable y_h to be substantially smaller than y_e, while $y_e \sim y_h$ is expected for NC DIS events.

Fig. 7a shows the distribution of $y_e \times (y_e - y_h)$ for the 214 events accepted by the preselection requirements and for the SM expectation. The hatched histogram shows how this variable would be distributed for events induced by a squark decaying via S8e. The thick line indicates the cut which is applied. This cut corresponds to a y_e dependent upper cut on $\sum(E - p_z)$ and has been optimised to maximise the signal significance. Fig. 7b and c show how this cut, indicated by the thick curves, discriminates between SUSY and NC DIS events, in the $(\sum(E - p_z), y_e)$ plane.

One candidate is observed in the data when applying the selection criteria listed above, in good agreement with the SM expectation of 3.2 ± 1.2 events, all coming from NC DIS processes.

The above requirements ensure a typical selection efficiency of $\sim 30\%$ on the searched signal.

5.4 Selection for ν + jets + X topologies

Two channels are considered to cover cases where squarks undergo a gauge decay leading to a neutrino instead of a positron in the final state. These final states, S5 and S8μ, are characterized by several jets and missing P_T and are selected by the following requirements :

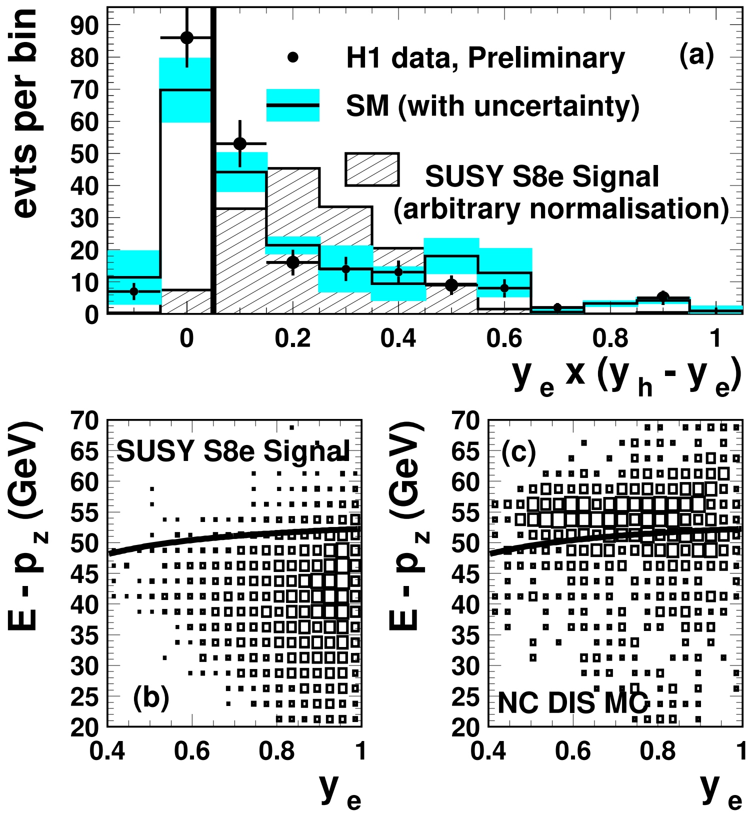

Figure 7: *(a) Distributions of the variable $y_e \times (y_e - y_h)$ for the 214 events satisfying the preselection criteria (symbols) and for the expectation from NC DIS and γp processes (white histogram). The gray error band on the white histogram indicates the uncertainty on the SM prediction. The hatched histogram shows how this variable is typically distributed for events coming from a squark decaying via S8e. The thick line shows the lower cut applied. Correlation of $\sum(E - p_z)$ and y_e for signal (b) and NC DIS (c) events. The cut applied is indicated in this plane by the thick curve.*

1. a transverse missing momentum $P_{T,miss} > 25$ GeV;
2. at least two jets in the angular range $7° < \theta < 145°$ and with $E_T > 10$ GeV, with the highest P_T jet satisfying $\theta > 10°$ and $E_T > 15$ GeV. This cut is exactly the same as described in section 5.3.

We observe 44 events satisfying the above selection criteria, in good agreement with the SM prediction of 46.5 ± 6.9, mainly coming from CC DIS processes. Fig. 8a-c shows for these selected events the distributions of the transverse momenta of the two highest P_T jets and of the polar angle of the highest P_T jet. All distributions are well described by the SM expectation. The corresponding distributions expected from squarks decaying into $\nu + jets$ are also shown as shaded histograms, where several kinematic configurations have been merged. Assuming that all the missing energy is carried away by one neutrino only, it is possible to reconstruct the kinematics of this ν by exploiting the constraint : $(E - p_z)_{had} + (E - p_z)_\nu = 55$ GeV between the $(E - p_z)$ of the hadronic final state and that of the escaping neutrino. The four-vector of

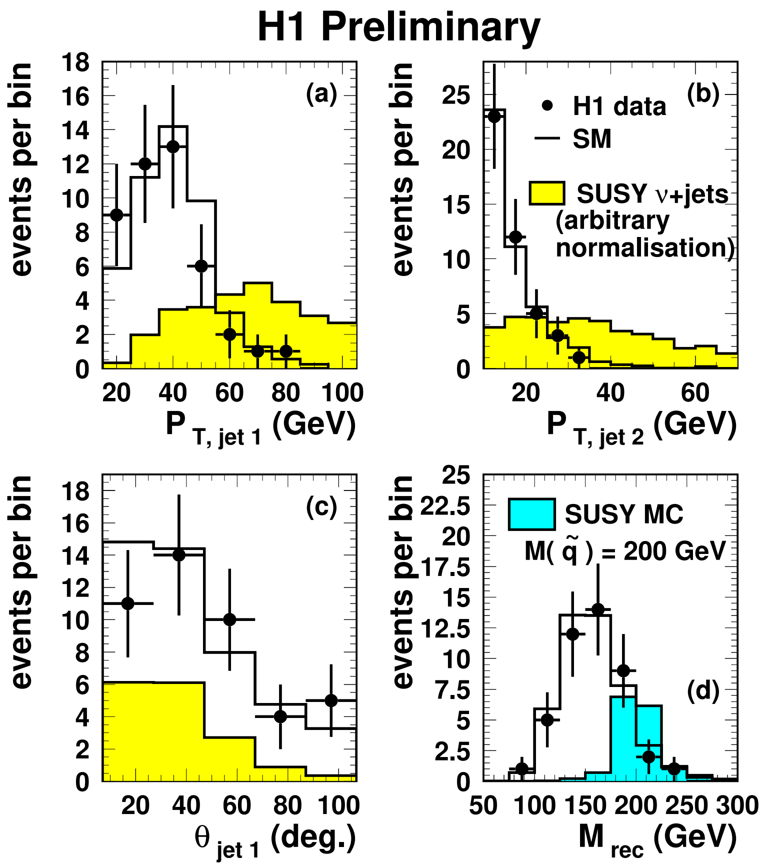

Figure 8: *For the ν + multijets $+X$ preselected events, observed (symbols) and expected (white histograms) distributions of the transverse momenta of the two highest P_T jets (a),(b), and the polar angle of the highest P_T jet (c). The shaded histograms show typical distributions of these variables for events coming from a squark decaying into $\nu + jets$. (d): The invariant mass M_{rec} in the centre of mass of the hard subprocess, assuming that only one neutrino escapes detection; M_{rec} should provide an estimate of the mass of a squark decaying via $S5$ into $\nu + jets$, as shown by the shaded histogram in (d) where the case of a 200 GeV squark has been considered.*

this ν is then added to that of the hadronic final state to reconstruct the invariant mass M_{rec} in the rest frame of the incoming electron and quark. The observed and expected distributions for M_{rec} are in good agreement as shown in Fig.8d. For squark decaying via the channel $\mathrm{S5}$, M_{rec} provides an estimate of the squark mass. The shaded histogram in Fig. 8d shows the resulting mass spectrum for Monte-Carlo events where a 200 GeV squark decays into $\nu + jets$. The observed resolution of ~ 40 GeV is typical for the range of squark masses probed in this analysis.

5.4.1 Event Selection for topology $\mathrm{S5}$

For squarks decaying via $\mathrm{S5}$ leading to ν + multijets final states, we apply a more stringent cut on the transverse momentum of the second highest P_T jet by requiring $P_{T,\mathrm{jet}\ 2} > 15$ GeV.

We observe 21 events satisfying these requirements, in very good agreement with the expectation of 22.9 ± 3.5 from SM processes.

The efficiency to select events induced by a squark decaying via $\mathrm{S5}$ ranges between $\sim 20\%$ and $\sim 60\%$.

5.4.2 Event Selection for topology $\mathrm{S8}$, μ channel ($\mathrm{S8}\mu$)

To search for gauge decays of squarks into neutrinos, a muon and several jets, the only requirement in addition to the common selection described above is the presence of a muon. The muon candidate is identified in the same way as for the channel $\mathrm{S7}\mu$ and has to fulfill the same criteria: $p_T^{\mu} > 5$ GeV and $10^{\circ} < \Theta < 110^{\circ}$. The selection efficiency for this $\mathrm{S8}\mu$ signal is typically $\sim 40\%$. No candidate is observed where 0.5 ± 0.2 are expected from SM processes, CC DIS being the dominantly contributing process.

5.5 Systematic Errors

In each channel analysed in the previous sections, the error on the mean expectation from Standard Model processes has been calculated by taking into account the systematic errors described below.
The experimental error sources considered are the following :

- the uncertainty of $\pm 1.5\%$ on the integrated luminosity which affects equally the SM expectations for each channel;
- the uncertainty on the absolute calibration of the calorimeters for electromagnetic energies, ranging between $\pm 0.7\%$ in the central wheels and $\pm 3\%$ in the forward region of the LAr calorimeter; this constitutes the main error source for the estimation of NC DIS background to channel $\mathrm{S1}$;
- the uncertainty of $\pm 4\%$ on the absolute hadronic energy scale. For inclusive or monojet NC DIS final states, the over-constrained kinematics allows to reduce this uncertainty to $\pm 2\%$ [18], which then applies to channels $\mathrm{S1}$ and $\mathrm{S2}$. This is the main error source for all considered channels but $\mathrm{S1}$.

The estimates of SM expectations also suffer from theoretical uncertainties which are summarized below :

- for NC DIS-like final states, the uncertainty of $\pm 5\%$ on parton density distributions obtained by QCD fits; for CC DIS-like topologies, which are mainly induced by d quarks whose density in the proton is less constrained, this uncertainty increases linearly with Q^2 up to $\simeq 20\%$ at the highest Q^2 considered here;
- the value of the strong coupling constant α_S, leading to an uncertainty of $\pm 4\%$;
- for channels $\mathrm{S1}$, $\mathrm{S3}$, $\mathrm{S4}$, $\mathrm{S7e}$ and $\mathrm{S8e}$, higher order QED corrections imply a $\pm 2\%$ uncertainty in the y range considered here.

All the analyses have been repeated with a shift of the central value of each of the sources of errors by ± 1 standard deviation to estimate their individual contribution. The overall systematic error on SM expectations is then determined as the quadratic sum of the resulting errors and of the statistical error on the Monte-Carlo simulation.

6 Results

Apart from a slight excess at $M_e \sim 200$ GeV in channel $\mathrm{S1}$, no significant deviation from the SM expectations has been found in the various $\not{R}_p$ and gauge decay channels analysed in section 5. Assuming that no signal has been observed (or, formally, that the observation contains at most two components, an unknown "resonance" signal and a known expectation from NC DIS), the various decay channels can be used and combined to set constraints on $\not{R}_p$ SUSY models.

As mentioned in section 2, when HERA operates with an incident beam of positrons, the best probed $\not{R}_p$ couplings are λ'_{1j1} which allow for resonant production of $\tilde{u}^j_L$ squarks. Hence we concentrate here on these λ'_{1j1} couplings, assuming one of them is non-vanishing for a given index j. In this section, mass dependent upper rejection limits on the Yukawa couplings λ'_{1j1} are first derived using, for each contributing channel, the branching ratios, the signal detection efficiencies and the numbers of observed and expected events. Limits are first derived in a "phenomenological" version of the MSSM where the masses of the sfermions are not related to the SUSY soft-breaking terms. Scans are performed in the framework this "phenomenological" MSSM as well as in the constrained MSSM, and conservative bounds on the Yukawa couplings are set in these models. Results are finally interpreted in the framework of the the so-called Minimal Supergravity (mSUGRA) model.

6.1 The Limits Derivation

We assume here that one of the λ'_{1j1} is non-vanishing and derive rejection limits on this coupling as a function of the $\tilde{u}^j_L$ mass, combining all contributing channels. As already mentioned before, gauge invariance forbids the $\tilde{u}^j_L$ to decay into $\nu + q$ and thus the channel $\mathrm{S2}$ is not considered in the limits derivation.

Mass dependent upper limits on the production cross section $\sigma(e^+ + p \rightarrow \tilde{u}^j_L)$ are obtained assuming Poisson distributions for the SM background expectations and for the signal. Each channel $\mathrm{S}k$ contributes in the limits derivation via its total branching ratio β_k, the numbers of observed and expected events satisfying $\mathrm{S}k$ selection cuts, and the corresponding selection efficiency. For channels $\mathrm{S1}$, $\mathrm{S3}$ and $\mathrm{S5}$, the numbers of observed and expected events are integrated within a mass bin which slides over the accessible mass range. The width of the mass bin is adapted to the expected mass resolution in each channel, so that this bin contains approximately 68% of the signal at a given squark mass. For example, the mass bins used to constrain a 200 GeV squark are $[186; 204]$ GeV and $[186; 206]$ GeV for $\mathrm{S1}$ and $\mathrm{S3}$ channels respectively. For channels $\mathrm{S4}$, $\mathrm{S7}$ and $\mathrm{S8}$, where both the expectation and the observation are small, no mass restriction is imposed.
Both systematic and statistical errors have been folded in channel by channel as described in [7].

The masses of the neutralinos and charginos, as well as the gauge couplings between any two SUSY particles and a standard fermion/boson, are determined by the usual MSSM parameters[6] : the "mass" term μ which mixes the Higgs superfields, the soft-breaking parameters M_1 and M_2 for $U(1)$ and $SU(2)$ gauginos, and the ratio $\tan\beta$ of the vacuum expectation values of the two neutral scalar Higgses. All these parameters are defined at the electroweak (EW) scale. We assume that the gaugino mass terms unify at the GUT scale to a common value $m_{1/2}$ leading

[6]The trilinear couplings between three scalar fields are neglected here.

to usual relations between M_1, M_2 and the $SU(3)$ soft breaking term M_3, and approximate the gluino mass by the value of M_3 at the EW scale.

For a fixed set of these MSSM parameters and specified values for the sfermions masses, the branchings β_k in the different channels Sk only depend on λ'_{1j1}[7]. This also holds for the upper limit on the cross section $\sigma_{lim}(\lambda')$ derived from the combination of the analysed channels. The upper limit on λ'_{1j1} at a given squark mass is then obtained by solving the equation : $\sigma_{lim}(\lambda') = \sigma(e^+p \to \tilde{u}^j_L)$ where the production cross section $\sigma(e^+p \to \tilde{u}^j_L)$ approximately scales with λ'^2_{1j1} but is calculated by taking into account the width of the resonant squark.

Decay chains involving more than two SUSY fermions (χ or $\tilde{g}$) can in principle contribute to the "gauge" channels analysed, and would lead to final states with very large jet multiplicities, for which the calculations of signal efficiencies are not straightforward. Hence, only cascades involving two SUSY fermions are taken into account in the calculation of the "observed" branching ratios into S3...S8. As an example, the total branching in channel S3 is determined as follows :

$$\begin{aligned} \beta_3 \;=\; & \sum_{X=\chi^0,\chi^+,\tilde{g}} \beta(\tilde{u}^j_L \to qX) \times \beta_X \\ + & \sum_{X=\chi^0,\chi^+,\tilde{g}} \beta(\tilde{u}^j_L \to qX) \times \sum_{Y=\chi^0,\chi^+,\tilde{g},M(Y)<M(X)} \beta(X \to qqY) \times \beta_Y \end{aligned}$$

where $\beta_{X,Y}$ represents the branching of $X, Y = \chi^0, \chi^+, \tilde{g}$ decaying via $\not{R}_p$ into e^+ + 2 jets. The decays $X \to qqY$ can be mediated by a real or virtual boson or sfermion. Radiative decays into the lightest Higgs boson h, e.g. $\chi^0_2 \to \chi^0_1 h$, can also contribute at low $\tan\beta$. Such decays, when followed by $h \to b\bar{b}$, are included in the calculation of the branching ratios β_k. The branching ratios for $\chi^0_\alpha \to \chi^0_\beta h$ depend a priori on another parameter determining the mass spectrum of the Higgs sector, taken here to be the pseudoscalar Higgs mass m_A. When m_A is not related to the other parameters it has been set to 300 GeV. Limits however do not depend on this assumption. The program HDECAY [36] has been used to determine the spectrum of the Higgs sector and the branching ratios of the Higgs bosons.

This determination of the branchings β_k is conservative, and it has been checked that, in the mass range considered here, the "observed" branching is generally close to 100%. The relevant decay widths of all involved sparticles have been obtained using the SUSYGEN package, taking into account all possible $\not{R}_p$ and gauge decays.

6.2 Limits on λ'_{1j1} in the "phenomenological" MSSM

We consider here a version of the MSSM where the parameters μ, M_2 and $\tan\beta$ are only used to determine the masses and couplings of the χ's, while the sfermions masses are free parameters. We assume that all squarks are degenerate. This assumption only enters in the calculation of the branching ratios of the χ's and of the gluino, since we are mainly probing the $\tilde{u}^j_L$ squark. Sleptons are also assumed degenerate, and their mass is set either to the common squark mass, or to a fixed value (90 GeV), close to the lowest mass bound coming from sfermions searches at LEP2.

[7]Same values for the branchings are then expected for $j = 1, 2$, while they differ a priori in the case of stop production ($j = 3$) due to the large top mass suppressing $\tilde{t} \to t\chi^0$ or $\tilde{t} \to t\tilde{g}$ decays.

Rejection limits obtained at the 95% confidence level (CL) on λ'_{1j1} ($j = 1, 2$) as a function of the $\tilde{u}^j_L$ mass are shown in Fig. 9a as the full (dashed) curve, under the assumption $M_{\tilde{l}} = 90$ GeV ($M_{\tilde{l}} = M_{\tilde{q}}$). Domains above the curves are excluded. The MSSM parameters have here been set to $\mu = -200$ GeV, $M_2 = 80$ GeV and $\tan\beta = 2$. With this choice of parameters, the lightest neutralino χ^0_1 is mainly dominated by its photino component and its mass is about 40 GeV, while the χ^+_1 and χ^0_2 are nearly degenerate around 90 GeV. It is worthwhile to note that combining all the contributing channels improves the sensitivity considerably, up to a factor $\simeq 5$ at lowest masses, compared to what would be achieved using only the $e + q$ data (i.e. channel $\mathrm{S1}$). The relative contributions of all channels are shown in Fig. 9b and Fig. 9c against the squark mass, at the current sensitivity limit on the Yukawa coupling, under the assumption $M_{\tilde{l}} = M_{\tilde{q}}$ and $M_{\tilde{l}} = 90$ GeV respectively. Assuming $M_{\tilde{l}} = M_{\tilde{q}}$, channels $\mathrm{S3}$ and $\mathrm{S4}$ have similar dominant contributions for masses up to $\simeq 230$ GeV. Only at the largest masses, where a large Yukawa

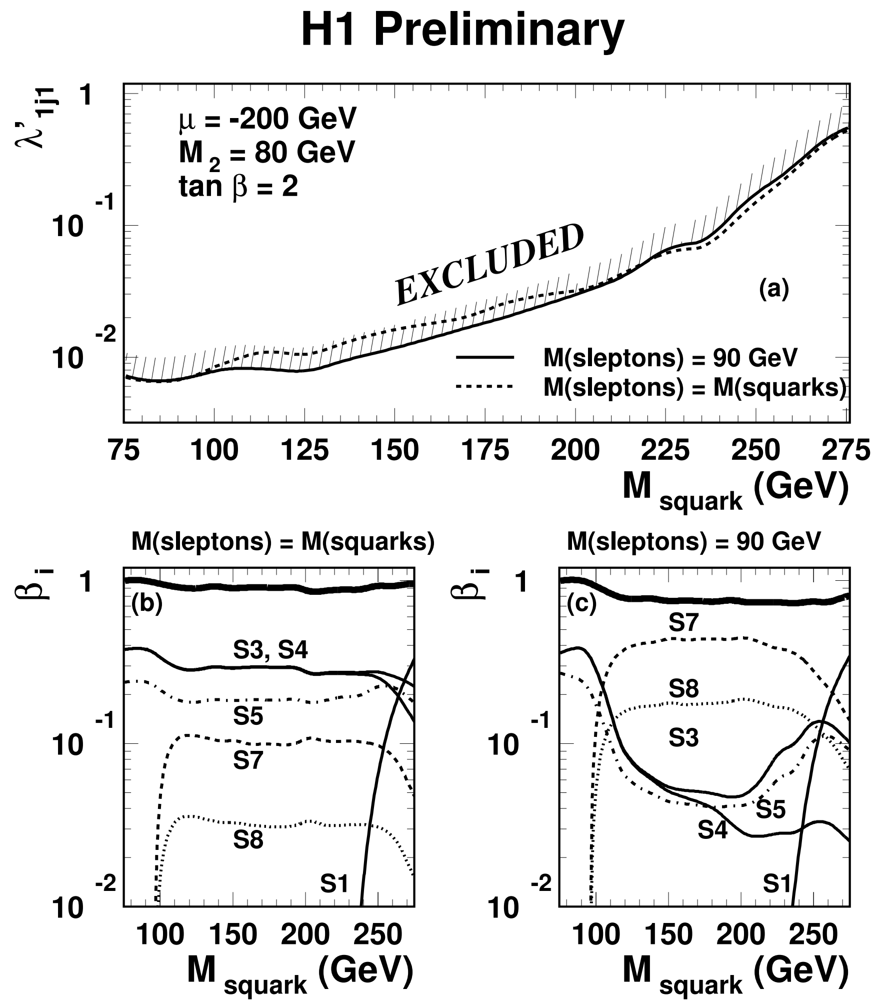

Figure 9: *(a): Exclusion upper limits at 95% CL for the coupling λ'_{1j1} as a function of the squark mass, for a set of MSSM parameters leading to a ~ 40 GeV χ^0_1 dominated by its photino component. Regions above the curves are excluded. The limits are given for two hypotheses on the slepton mass. (b): The relative contributions of all channels versus the squark mass, when sleptons and squarks are assumed to be degenerate; (c) : as (b) but assuming a slepton mass of 90 GeV. The thick curves in (b) and (c) indicate the total branching "seen" by the analysis.*

coupling is necessary to allow squark production, the increasing direct $R\!\!\!/_p$ decay of the χ_1^+ into e^+ + jets enhances the S3 contribution compared to that of S4. The contribution of S5 is significantly smaller, as expected since the χ_1^0 dominated by its photino component decays mainly into $e^\pm$ + jets. In the very high mass domain where the coupling probed λ becomes large, the relative contribution of S1 is largely enhanced.

The relative contribution of the different channels is significantly different when $M_{\tilde{l}} = 90$ GeV is assumed, as can be seen in Fig. 9c. As in the previous case, S3 and S4 dominate in the lowest squark mass domain, but become sub-leading as soon as the squark decays into χ_1^+ or χ_2^0 are kinematically allowed. Indeed the subsequent decay of χ_1^+ or χ_2^0 mainly proceeds via a two-body decay mode into a lepton-slepton pair, mostly followed by a decay of the slepton into χ_1^0. As a result, the contributions of the channels S7 and S8 are considerably enhanced. This remains the case when the decays of the χ's proceed via a slightly off-shell slepton. S7

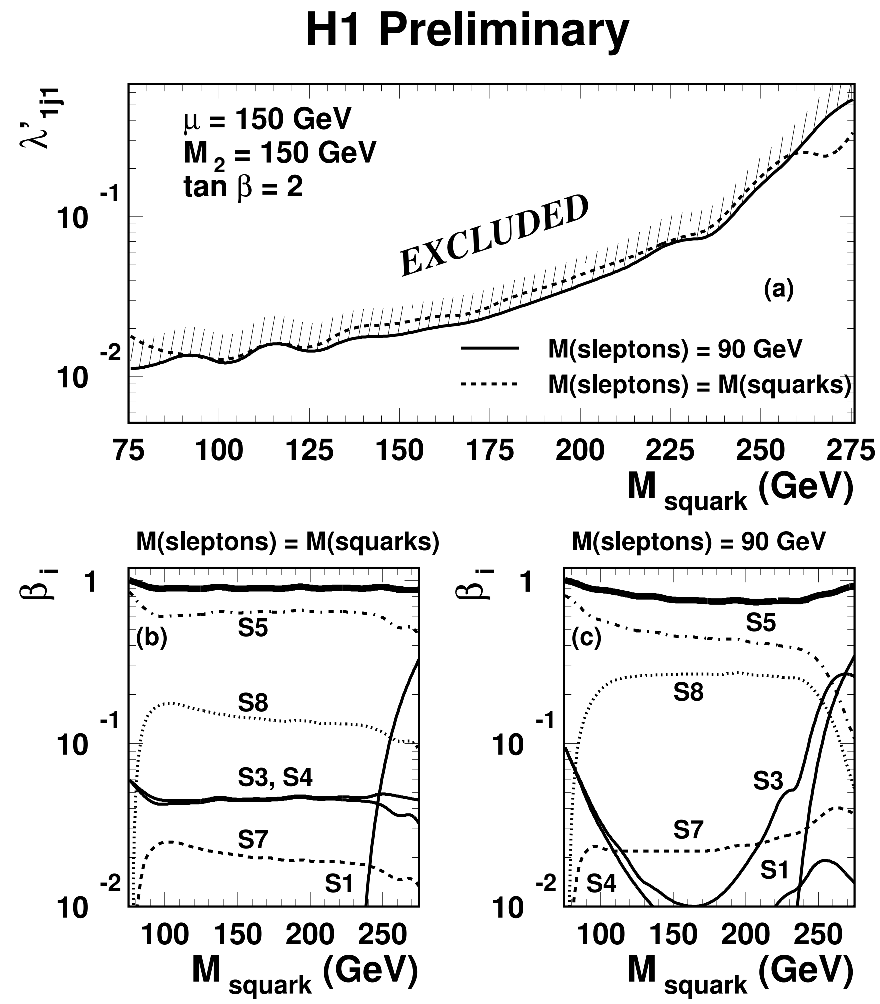

Figure 10: *(a): Exclusion upper limits at* 95% *CL for the coupling* λ'_{1j1} *as a function of the squark mass, for a set of MSSM parameters leading to a* ~ 40 GeV χ_1^0 *dominated by its zino component. Regions above the curves are excluded. The limits are given for two hypotheses on the slepton mass. (b): The relative contributions of all channels versus the squark mass, when sleptons and squarks are assumed to be degenerate; (c): as (b) but assuming a slepton mass of 90 GeV. The thick curves in (b) and (c) indicate the total branching "seen" by the analysis.*

contributes more than S8 since the χ_1^0 mainly decays into $e^{\pm}$ and jets. S3 has a larger contribution than S4 due to decays $\chi_1^+ \rightarrow \tilde{\nu}_e e^+$ followed by a $\not R_p$decay of the sneutrino into two jets. Since the sensitivity of our analysis is similar in all gauge channels, the upper limits on the Yukawa coupling are close to those obtained assuming $M_{\tilde{l}} = M_{\tilde{q}}$. Not including the channels S7 and S8 would significantly hamper the limit, by a factor ~ 2 for squark masses between ~ 100 GeV and ~ 230 GeV.

Similar results are shown in Fig. 10 for a set of values for $(\mu, M_2, \tan\beta)$ leading to a 40 GeV χ_1^0 dominated by its zino component. As expected, S5 is now the dominant channel since the zino-dominated χ_1^0 mainly decays into ν + jets. This remains the case under the assumption that $M_{\tilde{l}} = 90$ GeV because the χ_1^+ is here slightly lighter than 90 GeV. However decays of the χ_1^+ into a slightly off-shell slepton lead to the enhancement of the channel S8, as seen in Fig. 10c.

For the two sets of MSSM parameters chosen in Fig. 9 and Fig. 10, the gluino mass is large due to the large M_2 values and thus squark decays into $\tilde{g}$ are not kinematically allowed. Moreover radiative decays of heavy neutralinos into the light Higgs h are only important for the χ_3^0, and decays of the $\tilde{u}_L^j$ into this neutralino are strongly suppressed due to the Higgsino dominance of the χ_3^0 in these example cases.

In order to allow a more systematic study of the dependence of our sensitivity on the MSSM parameters, a scan on the MSSM parameters M_2 and μ is performed, for $\tan\beta = 2$. The mass of the sleptons is set to 90 GeV. The parameters M_2 and μ are varied in the range 70 GeV $< M_2 <$

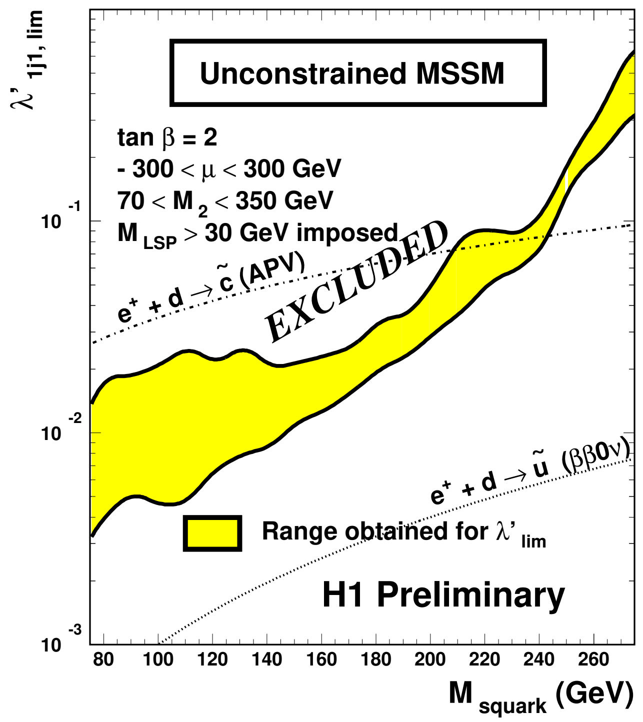

Figure 11: *Exclusion upper limits at 95% CL on the coupling λ'_{1j1} as a function of the squark mass for $\tan\beta = 2$, in the "phenomenological" MSSM. For each squark mass, a scan on the MSSM parameters M_2 and μ has been performed and the largest (lowest) value for the coupling limit is shown by the upper (lower) curve.*

300 GeV and -300 GeV $< \mu <$ 300 GeV. Points which lead to a scalar LSP or to a LSP mass below 30 GeV are not considered. This latter restriction, as well as the lowest allowed value for M_2, are motivated by the exclusion domains resulting from χ's searches in $\not{R}_p$SUSY carried out by the LEP2 experiments. For each point in this (μ, M_2) grid the upper bound λ'_{lim} on the coupling λ'_{1j1} is obtained as explained above. The most extreme curves in Fig.11 indicate the maximal and minimal values obtained for λ'_{lim} as a function of the squark mass, for $\tan\beta = 2$.

The spread of the domain spanned by the limits on the Yukawa coupling is not too large and decreases with increasing squark mass. Less favourable cases occur when the squark dominantly decays via the channel S5, for which the large $P_{T,miss}$ requirement induces an efficiency loss especially for low squark masses. In addition, unfavourable situations might occur when large higgsinos components of the involved neutralinos lead to an enhancement of the decay $\chi_2^0 \rightarrow \chi_1^0 \tau^+ \tau^-$, which are not taken into account in the analysis. The sensitivity of our limits on the parameter $\tan\beta$ is studied in the next section.

Our results are also compared in Fig. 11 to the most stringent indirect limits. The production of a $\tilde{u}$ squark via a λ'_{111} coupling is very severely constrained by the non-observation of neutrinoless double beta decay [37] as shown by the dotted curve. The most severe indirect limit on the coupling λ'_{121}, which could allow for the production of squarks $\tilde{c}$, comes from Atomic Parity Violation [38, 39] and is indicated by the dashed curve in Fig. 11. For squark masses below $\sim$ 240 GeV H1 direct limits significantly improve this indirect constraint on λ'_{121} by a factor up to $\simeq 3$.

6.3 Limits on λ'_{1j1} in the constrained MSSM

In this section we consider a "constrained" version of the MSSM where the number of free parameters is reduced. In addition to the GUT relation mentioned above relating M_1, M_2 and M_3, we assume a universal mass parameter m_0 for all sfermions at very high scale. The evolution of the sfermions masses towards low scales is then driven by the Renormalisation Group Equations (RGE) and depends on the gauge quantum numbers of the sfermions. As a result, the sfermions masses at the electroweak scale are related to each other and to the parameters determining the gaugino sector. The model is thus completely determined by e.g. m_0, M_2, μ and $\tan\beta$ (m_A is set to 300 GeV as already mentioned, and we assume no mixing between the sfermions at the electroweak scale).

For a given value of the $\tilde{u}_L^j$ squark mass, the requirement of sfermions unification at large scale imposes an upper bound on the parameter M_2, which is obtained using approximate solutions for the RGE. This upper bound on M_2 increases with the squark mass. We then perform a scan on μ (-300 GeV $< \mu <$ 300 GeV), $\tan\beta$ ($2 \leq \tan\beta \leq 40$), and on M_2 in its allowed range defined by $M(\tilde{u}_L^j)$ and $\tan\beta$. As before points leading to a scalar LSP or to a LSP mass below 30 GeV are not considered. This lower bound on the LSP mass forbids too small values of M_2 and hence imposes a lower bound on the $\tilde{u}_L^j$ mass.

The most extreme curves in Fig.12 indicate the maximal and minimal values obtained for λ'_{lim} as a function of the $\tilde{u}_L^j$ mass ($j = 1, 2$). It can be seen that the spread of the domain spanned by the limits λ'_{lim} is quite small, i.e. that the sensitivity of our analysis on λ' does not depend too much on the free parameters of the model. The most optimistic limits are usually obtained for large $\tan\beta$ and are in general better than those derived previously in the "unconstrained" MSSM where only large values of M_2 were considered. Indeed, for moderate values of M_2 and

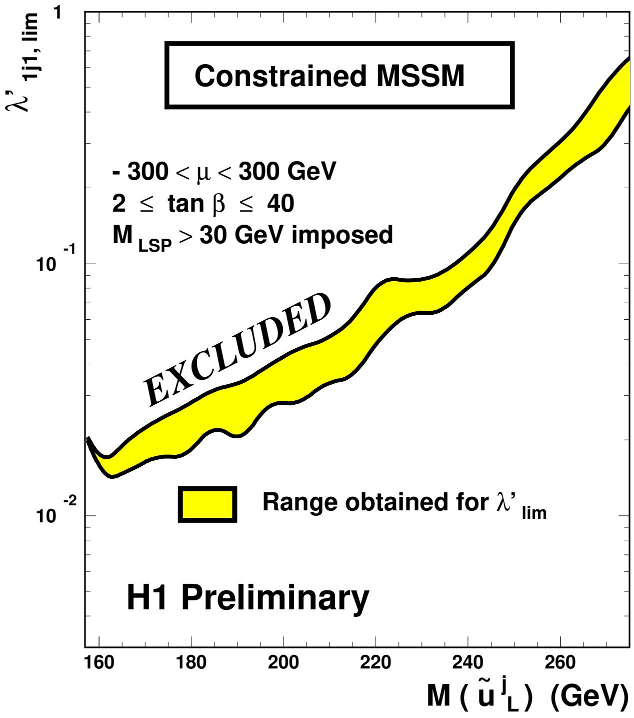

Figure 12: *Exclusion upper limits at 95% CL for the coupling λ'_{1j1} as a function of the mass of the $\tilde{u}^j_L$ ($j = 1, 2$), in the constrained MSSM. For each squark mass, a scan on the MSSM parameters μ, M_2 and $\tan\beta$ has been performed and the largest (smallest) value for the coupling limit is shown by the upper (lower) curve.*

large $\tan\beta$, the sneutrinos are very light, leading to an enhancement of the quasi background-free channels $\mathrm{S7}$ and $\mathrm{S8}$ via $\chi^+_1 \rightarrow l^+\tilde{\nu}$. On the other hand, the smallest sensitivities on the Yukawa coupling are obtained either when $\mathrm{S5}$ dominates, or when the gluino is light enough so that $\tilde{u}_L \rightarrow u\tilde{g}$ is the dominant decay mode, and when the coupling of the χ^0_1 to "right"-squarks is suppressed (i.e. when χ^0_1 is dominated by its zino or higgsinos components). In this latter case the main decay mode of the $\tilde{g}$ proceeds via an heavier χ. Such cascade decays of squarks, involving more than two SUSY fermions, are not taken into account as already mentioned.

For a Yukawa coupling of the electromagnetic strength ($\lambda'_{1j1} = 0.3$), squark masses up to values between 258 and 267 GeV can be ruled out at 95% CL in the framework of the constrained MSSM. This extends far beyond the mass domain excluded from relevant searches for scalar leptoquarks performed by both the $D\emptyset$ [3] and CDF [4] experiments at the TeVatron collider. These rule out $\tilde{u}^j_L$ squark masses below 205 GeV as soon as the branching ratio of the squark into $e^+ + q$ is greater than $\simeq 50\%$, but the excluded mass domain does not extend above $\simeq 110$ GeV for values of this branching below 10%. Since in $\not{R}_p$ SUSY such a branching can be naturally small as seen in section 6.2 such leptoquark-like constraints are easily evaded. Comparisons with specific $\not{R}_p$SUSY searches carried out at the TeVatron will be addressed in the next section. Moreover, for a coupling strength ten times smaller than α_{EM}, the most conservative bound on the mass of the $\tilde{u}^j_L$ obtained from this analysis still reaches 182 GeV.

6.4 Limits on λ'_{1j1} in mSUGRA

The model considered previously can still be more constrained by imposing that the breaking of the electroweak symmetry is driven by radiative corrections, leading to the so-called mSUGRA model. Requiring the Radiative Electroweak Symmetry Breaking (REWSB), the equations corresponding to the minimisation of the Higgs potential allow to express $|\mu|$ as a function of the other parameters. Only the sign of μ remains arbitrary. The program SUSPECT 1.2 [40] is used to obtain the REWSB solution for $|\mu|$ when the other parameters are fixed. It makes use of a Runge-Kutta algorithm to solve numerically the one-loop RGE.

Assuming a fixed value for the $R\!\!\!/_p$ coupling λ'_{1j1} ($j = 1, 2$), our negative searches can be expressed in terms of constraints on the mSUGRA parameters, for example on $(m_0, m_{1/2})$ when $\tan\beta$, the common trilinear coupling A_0 and the sign of μ are fixed. Values of the parameters leading to a LSP lighter than 30 GeV have not been excluded here. However a vanishing efficiency has been assumed for squarks undergoing a gauge decay ending by a SUSY fermion lighter than 30 GeV, since efficiencies in this mass domain have not been calculated (see section 4).

For $\tan\beta = 2$, $A_0 = 0$ and $\mu < 0$, results obtained for a Yukawa coupling $\lambda'_{1j1} = 0.3$ are shown in Fig. 13a. The obtained limit basically follows the squark mass isoline $M(\tilde{u}^j_L) \sim$

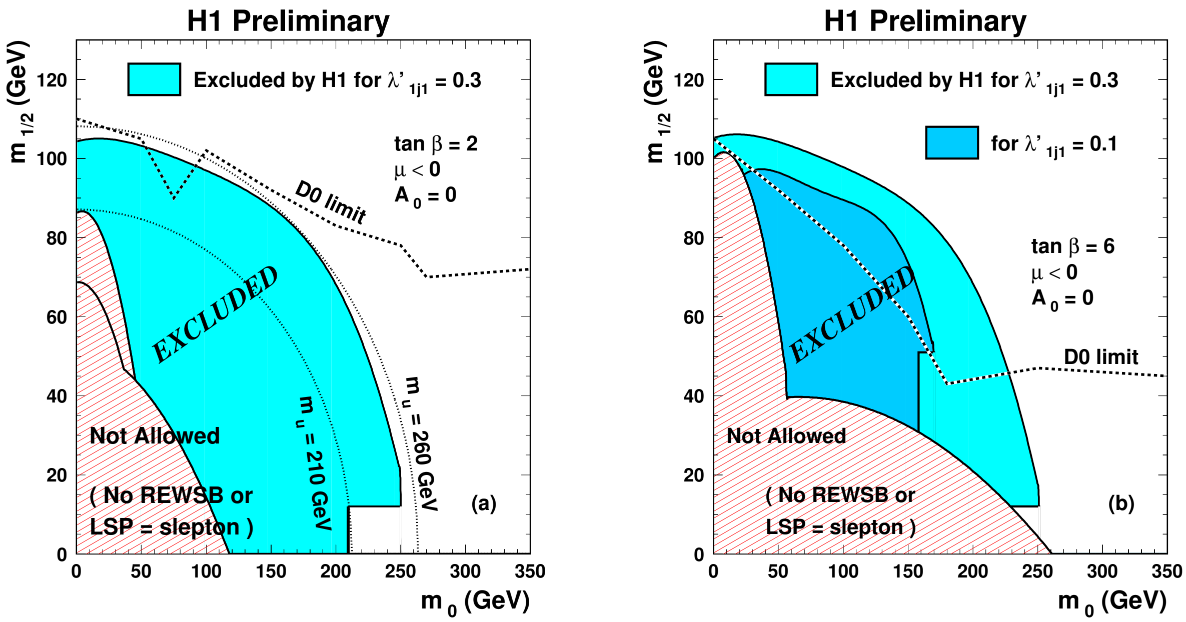

Figure 13: *Domain of the plane $(m_0, m_{1/2})$ excluded by this analysis for $\mu < 0$, $A_0 = 0$ and $\tan\beta = 2$ (a), and $\tan\beta = 6$ (b), for a $R\!\!\!/_p$coupling $\lambda'_{1j1} = 0.3$ (light shaded areas). In (b) the exclusion domain obtained for $\lambda'_{1j1} = 0.1$ is also shown as the dark gray area. The hatched domains correspond to values of the parameters where no REWSB is possible or where the LSP is a sfermion. The region below the dashed curves is excluded by the $D\emptyset$ experiment. Two isolines for the mass of the $\tilde{u}^j_L$ are also shown in (a) as dotted curves.*

260 GeV. At low $m_{1/2}$ value, the sensitivity is however decreased down to $M(\tilde{u}^j_L) \sim 210$ GeV due to the important branching ratio of the squark in cascade decays involving a very light (< 30 GeV) SUSY fermion, for which the efficiency has been conservatively set to zero. The region of the $(m_0, m_{1/2})$ plane below the dashed curve is excluded from searches for SUSY where R_p is violated by a λ'_{1jk} coupling carried out at the $D\emptyset$ experiment [41], relying on dielectrons events. HERA and TeVatron sensitivities are quite similar in the low m_0 domain, but at larger m_0 HERA's sensitivity decreases due to the increasing squark mass, while sensitivity is still obtained in $p\bar{p}$ collisions via gluino production.

Similar results are shown in Fig. 13b for $\tan\beta = 6$. The domains excluded by this analysis are shown for $\lambda'_{1j1} = 0.3$ ($\lambda'_{1j1} = 0.1$) as the light shaded (dark shaded) areas. For such large values of $\tan\beta$ the domain probed by this analysis considerably extends beyond the region excluded by the $D\emptyset$ experiment. This is due to the fact that, for large values of $\tan\beta$, the lightest neutralino is dominated by its zino component, so that its decay into $e^{\pm}$ is suppressed. As a result the sensitivity of the $D\emptyset$ analysis using the dielectron channel is decreased, while the dominant squark decay mode is still "seen" in the H1 analysis via the $\mathsf{S5}$ and $\mathsf{S8}$ channels.

7 Conclusions

We have searched for resonant squarks in ep collisions at HERA in R-parity violating as well as gauge decay modes. No significant evidence for the production of squarks was found and mass dependent limits on the R-parity violating couplings were derived. In the MSSM framework, the existence of squarks coupling to a e^+d pair with masses up to 182 GeV $(258$ GeV$)$ is excluded at 95% confidence level for a strength of the Yukawa coupling equal to $0.01 \times \alpha_{em}$ (α_{em}), independently of the values of the model parameters. For the first time at HERA, results have been interpreted in the framework of the Minimal Supergravity Model. Our limits extend beyond the domain covered by other collider experiments especially at large $\tan\beta$.

Acknowledgements

We wish to thank the HERA machine group as well as the H1 engineers and technicians who constructed and maintained the detector for their outstanding efforts. We thank the funding agencies for their financial support. We wish to thank the DESY directorate for the support and hospitality extended to the non-DESY members of the collaboration.

References

[1] H1 Collaboration, C. Adloff *et al.*, Z. Phys. C74 (1997) 191.

[2] ZEUS Collaboration, J. Breitweg *et al.*, Z. Phys. C74 (1997) 207.

[3] D∅ Collaboration, B. Abbott *et al.*, Phys. Rev. Lett. 79 (1997) 4321;
idem, Phys. Rev. Lett. 80 (1998) 2051.

[4] CDF Collaboration, F. Abe *et al.*, Phys. Rev. Lett. 79 (1997) 4327.

[5] CDF and $D\emptyset$ Collaborations, "Combined Limits on First Generation Leptoquarks from the CDF and $D\emptyset$ Experiments", hep-ex/9810015, Oct. 1998, 9pp.

[6] D. Choudhury and S. Raychaudhuri, Phys. Lett. B401 (1997) 54; G. Altarelli *et al.*, Nucl. Phys. B506 (1997) 3; H. Dreiner and P. Morawitz, Nucl. Phys. B503 (1997) 55; T. Kon and T. Kobayashi, Phys. Lett. B409 (1997) 265; G. Altarelli, G.F. Giudice and M.L. Mangano, Nucl. Phys. B506 (1997) 29; J. Ellis, S. Lola, K. Sridhar, Phys. Lett. B408 (1997) 252; J.E. Kim and P. Ko, Phys. Rev. D57 (1998) 489; S. Lola, Proceed. of the 5th Int. Workshop on Deep Inelastic Scattering and QCD, Chicago, USA, (April 14-18, 1997) 5pp.; G. Altarelli, Proceedings of the SUSY 1997 Conference, Nucl. Phys. Proc, Suppl. 62 (1998) 3; R. Rückl, H. Spiesberger, Proceed. of the Workshop New Trends in HERA Physics, Tegernsee, Germany (May 25-30,1997) 14pp.; A. S. Joshipura, V. Ravindran and S. K. Vempati, Phys. Rev. D57 (1998) 5327; J. Ellis, Proceed. of the Europhysics Conf. on High-Energy Physics, Jerusalem (August 1997) 8pp.; S. Raychaudhuri, Proceed. of the Int. Workshop on Physics Beyond the Standard Model, Valencia, Spain (October 13 - 17, 1997) 5pp.; E. Asakawa, J. Kamoshita and A. Sugamoto, Ochanumizu Univ. preprint PP-115 (March 1998) 15pp..

[7] H1 Collaboration, T. Ahmed *et al.*, Z. Phys. C64 (1994) 545.

[8] H1 Collaboration, S. Aid *et al.*, Z. Phys. C71 (1996) 211.

[9] H1 Collaboration, ICHEP'98 Contrib. Paper 580.

[10] J. Butterworth and H. Dreiner, Nucl. Phys. B397 (1993) 3, and references therein.

[11] H1 Collab., Eur.Phys.J. C11 (1999) 447.;

[12] W. Buchmüller, R. Rückl and D. Wyler, Phys. Lett. B191 (1987) 442. *Erratum* Phys. Lett. B448 (1999) 320.

[13] DELPHI Collab., EPS'99 Contrib. paper 431.

[14] H1 Collaboration, I. Abt *et al.*, DESY preprint 93-103 (July 1993) 194pp.; *idem* DESY Internal Report H1-96-01 (March 1996) 157pp.; *idem* Nucl. Instr. and Meth. A386 (1997) 310.

[15] H1 Calorimeter Group, B. Andrieu *et al.*, Nucl. Instr. and Meth. A336 (1993) 460.

[16] H1 Calorimeter Group, B. Andrieu *et al.*, Nucl. Inst. and Meth. A344 (1994) 492.

[17] H1 Calorimeter Group, B. Andrieu *et al.*, Nucl. Instr. and Meth. A350 (1994) 57; *idem*, Nucl. Instr. and Meth. A336 (1993) 499.

[18] H1 Collaboration, C. Adloff *et al.*, Eur. Phys. J. C13 (2000) 609.

[19] H1 SPACAL Group, R.D. Appuhn *et al.*, Nucl. Instr. and Meth. A386 (1997) 397.

[20] H1 BEMC Group, J. Ban *et al.*, Nucl. Instr. and Meth. A372 (1996) 399.

[21] DJANGO 2.1; G.A. Schuler and H. Spiesberger, Proceedings of the Workshop Physics at HERA, W. Buchmüller and G. Ingelman (Editors), (October 1991, DESY-Hamburg), vol. 3 p. 1419.

[22] HERACLES 4.4; A. Kwiatkowski, H. Spiesberger and H.-J. Möhring, Comput. Phys. Commun. 69 (1992) 155.

[23] G. Gustafson and U. Pettersson, Nucl. Phys. B306 (1988) 746; *idem*, *addendum* Lund University preprint LU-TP-87-19, (October 1987) 4pp.; B. Andersson *et al.*, Z. Phys. C43 (1989) 625.

[24] ARIADNE 4.0; L. Lönnblad, Comput. Phys. Commun. 71 (1992) 15.

[25] JETSET 7.4; T. Sjöstrand, Lund Univ. preprint LU-TP-95-20 (August 1995) 321pp; *idem*, CERN preprint TH-7112-93 (February 1994) 305pp.

[26] A.D. Martin, R.G. Roberts, W.J. Stirling and R.S. Thorne, Euro. Phys. J. C4 (1998) 463.

[27] PYTHIA 5.7; T. Sjöstrand, CERN-TH-6488 (1992), Comp. Phys. Comm. 82 (1994) 74.

[28] M. Glück, E. Reya and A. Vogt, Phys. Rev. D45 (1992) 3986; *idem*, Phys. Rev. D46 (1992) 1973.

[29] LEGO 0.02 and SUSSEX 1.5; K. Rosenbauer, PhD. thesis, RWTH Aachen (in German), PITHA 95/16 (July 1995).

[30] H1 Collaboration, I. Abt *et al.*, Nucl. Phys. B396 (1993) 3; *idem*, T. Ahmed *et al.*, Z. Phys. C64 (1994) 545; *idem*, T. Ahmed *et al.*, Phys. Lett. B369 (1996) 173.

[31] SUSYGEN 2.2, "A Monte Carlo Event Generator for MSSM Sparticle Production at e^+e^- Colliders", S. Katsanevas and P. Morawitz, Comp. Phys. Comm. 112 (1998) 227. (hep-ph/9711417).

[32] SUSYGEN 3.0/0.6, "A Monte Carlo Event generator for MSSM sparticle production for e^+e^-, $\mu^+\mu^-$ and ep colliders", N. Ghodbane, S. Katsanevas, P. Morawitz and E. Perez, http://lyoinfo.in2p3.fr/susygen/susygen3.html.

[33] E. Perez, Proceedings of the Workshop "Monte-Carlo Generators for HERA Physics", DESY, 1998-1999, p 635, A.T. Doyle, G. Grindhammer, G. Ingelman and H. Jung (Editors).

[34] V.N. Gribov et L.N. Lipatov, Sov. Journ. Nucl. Phys. 15 (1972) 78;
G. Altarelli et G. Parisi, Nucl. Phys. B126 (1977) 298;
Y.L. Doskhitzer, JETP 46 (1977) 641.

[35] A. Blondel, F. Jacquet, Proceedings of the Study of an ep Facility for Europe, ed. U. Amaldi, DESY report 79-48 (1979) 391.

[36] HDECAY, A. Djouadi, J. Kalinowski and M. Spira, hep-ph/9704448 (April 97)

[37] R. Mohapatra, Phys. Rev. D34 (1986) 3457; J.D. Vergados, Phys. Lett. B184 (1987) 55.;
M. Hirsch, H.V. Klapdor-Kleingrothaus, S.G. Kovalenko, Phys. Lett. B352 (1995) 1.
M. Hirsch, H.V. Klapdor-Kleingrothaus, S.G. Kovalenko, Phys. Rev. Lett. 75 (1995) 17; Phys. Rev. D53 (1996) 1239.

[38] P. Langacker, Phys. Lett. B256 (1991) 277.

[39] H. Dreiner, to be published in "Perspectives on Supersymmetry", Ed. G.L. Kane, World Scientific, hep-ph/9707435, 18pp.

[40] SUSPECT 1.2, code written by A. Djouadi, J.L. Kneur and G. Moultaka.

[41] $D\emptyset$ Collaboration, B. Abbott et al., Phys. Rev. Lett. 83 (1999) 4476.